Temporal metabolic profiling of the *Quercus suber–Phytophthora cinnamomi* system by middle-infrared spectroscopy

By P. R. Hardoim[1,2,7], R. Guerra[3], A. M. Rosa da Costa[2], M. S. Serrano[4], M. E. Sánchez[5] and A. C. Coelho[3,6]

[1]CCMAR – Centre of Marine Sciences, University of Algarve, Campus Gambelas, 8005-139 Faro, Portugal; [2]CIQA – Algarve Chemistry Research Centre and Department of Chemistry and Pharmacy, Faculty of Sciences and Technology, University of Algarve, Campus Gambelas, 8005-139 Faro, Portugal; [3]CEOT – Centro de Eletrónica Optoeletronica e Telecomunicações, University of Algarve, Faro, Portugal; [4]Forest Pathology and Mycology Laboratory, University of California, Berkeley, CA, USA; [5]Patología Agroforestal, University of Córdoba, Córdoba, Spain; [6]University of Algarve, Faro, Portugal; [7]E-mail: phardoim@gmail.com (for correspondence)

Summary

The oomycete *Phytophthora cinnamomi* is an aggressive plant pathogen, detrimental to many ecosystems including cork oak (*Quercus suber*) stands, and can inflict great losses in one of the greatest 'hotspots' for biodiversity in the world. Here, we applied Fourier transform-infrared (FT-IR) spectroscopy combined with chemometrics to disclose the metabolic patterns of cork oak roots and *P. cinnamomi* mycelium during the early hours of the interaction. As early as 2 h post-inoculation (hpi), cork oak roots showed altered metabolic patterns with significant variations for regions associated with carbohydrate, glycoconjugate and lipid groups when compared to mock-inoculated plants. These variations were further extended at 8 hpi. Surprisingly, at 16 hpi, the metabolic changes in inoculated and mock-inoculated plants were similar, and at 24 hpi, the metabolic patterns of the regions mentioned above were inverted when compared to samples collected at 8 hpi. Principal component analysis of the FT-IR spectra confirmed that the metabolic patterns of inoculated cork oak roots could be readily distinguished from those of mock-inoculated plants at 2, 8 and 24 hpi, but not at 16 hpi. FT-IR spectral analysis from mycelium of *P. cinnamomi* exposed to cork oak root exudates revealed contrasting variations for regions associated with protein groups at 16 and 24 h post-exposure (hpe), whereas carbohydrate and glycoconjugate groups varied mainly at 24 hpe. Our results revealed early alterations in the metabolic patterns of the host plant when interacting with the biotrophic pathogen. In addition, the FT-IR technique can be successfully applied to discriminate infected cork oak plants from mock-inoculated plants, although these differences were dynamic with time. To a lesser extent, the metabolic patterns of *P. cinnamomi* were also altered when exposed to cork oak root exudates.

1 Introduction

Cork oak (*Quercus suber* L.) is an evergreen tree, autochthonous to the Mediterranean Basin, with the largest continuous area located in the Iberian Peninsula (Bugalho et al. 2011). The cork oak savanna-like ecosystem (cork oak *montado*) is characterized by low-density tree stands that support one of the world's greatest 'hotspots' for biodiversity (Myers et al. 2000). Therefore, the importance of cork oak savanna far exceeds the socio-economic values derived from its main product – cork. Nevertheless, land management of the *Quercus* spp. '*montado*' has been severely neglected in recent years (Pinto-Correia and Godinho 2013; Pinto-Correia et al. 2014). Several factors are constantly challenging this human-mediated ecosystem, including numerous biotic (e.g. pathogens, insects) and abiotic (e.g. waterlogging, drought, fire and soil organic matter depletion) factors (Robin et al. 2001; Corcobado et al. 2013, 2014). Among biotic factors, root rot disease caused by the oomycete *Phytophthora cinnamomi* (Rands) is most likely to be responsible for the progressive decline of Iberian cork oak stands (Brasier et al. 1993; Moreira and Martins 2005; Moralejo et al. 2009; Camilo-Alves et al. 2013). Large root losses were observed on 1-year-old cork oak seedlings inoculated with *P. cinnamomi*, which were further aggravated by waterlogging (Robin et al. 2001). Corcobado et al. (2014) observed more severe damage on *Quercus ilex* caused by *P. cinnamomi* infection when seedlings were subjected to waterlogging followed by water deprivation.

Phytophthora cinnamomi is an aggressive soilborne pathogen that, once introduced into the ecosystem, causes significant changes in plant community structure, reducing biodiversity and threatening endemic plant species (Hardham 2005). It is believed to originate from South-East Asia (i.e. New Guinea, Malaysia), where it infects few host species (Brasier 2008). However, with its worldwide dissemination, this plant pathogen has been shown to infect over 3000 plant species, causing extensive economic losses in agriculture, horticulture and forestry alike (Hardham 2005). A wide range of physiological alterations is known to occur in plants in response to pathogen attack, including the production of reactive oxygen species (ROS), transient ion flux, cell wall strengthening, release of salicylic acid, jasmonic acid, ethylene and synthesis of pathogenesis-related proteins (Jones and Dangl 2006).

Recently, metabolomics studies have been applied to link genes to functions (Hall 2006). Metabolomics can be described as the study of all metabolites synthesized by a biological system. Among different metabolic approaches, metabolic profiling has appeared as a useful analytical tool to investigate plant–pathogen interactions (Fiehn 2002; Cameron et al. 2006). One of the metabolic profiling techniques, the Fourier transform-infrared (FT-IR) spectroscopy, has been applied successfully for differentiation of functional biochemical groups in plants challenged by abiotic perturbations and/or biotic interactions (Gidman et al. 2003; Martín et al. 2005; Martin et al. 2008; Conrad et al. 2014). However, because biological systems are composed of a myriad of polymers, macromolecules and metabolites, their infrared spectra are obviously highly

complex, comprising the relative contributions from different functional groups, chemical structures and their interactions (Kamnev et al. 1997). Despite its complexity, FT-IR spectral analysis of control and challenged samples allows associated bands to be assigned to the main functional groups present therein. Hence, although it is not possible to identify the structure, composition and absolute concentration of individual metabolites (i.e. fingerprinting), pattern recognition can be used to interpret biological interactions and metabolic alterations (i.e. profiling; Brereton 2009).

The main objective of this study was to identify patterns of metabolic changes in samples of cork oak roots inoculated with *P. cinnamomi* and samples of *P. cinnamomi* mycelium exposed to cork oak root exudates. Specifically, we addressed the following questions: (i) How does inoculation with *P. cinnamomi* affect the metabolic profile of cork oak roots? (ii) How does the metabolic profile of *P. cinnamomi* vary when exposed to cork oak root exudates? (iii) What are the dynamics of the responses? FT-IR spectroscopy (4000–400 cm^{-1}) was applied in a time series assay (i.e. 2, 8, 16, 24 h) to address these objectives.

2 Material and methods

2.1 Biological material

The patterns of metabolic profiling from two biological systems, cork oak roots and mycelium of *P. cinnamomi*, were investigated in a time series. For the interaction, two distinct biological assays were performed as follows: (i) the root assay, which accounted for the interaction between cork oak roots and zoospores of *P. cinnamomi* (ii) the mycelium assay, which accounted for the effect of cork oak root exudates on mycelium of *P. cinnamomi*. Mock-inoculated and mock-exposed samples were used as controls for cork oak root and mycelium of *P. cinnamomi*, respectively. Cork oak acorns were harvested from a single tree from Serra do Caldeirão, Algarve, Portugal, in October 2011 and stored in a dark chamber at 5°C until sown. To prevent root wounds, acorns were germinated on autoclaved moist paper towels and incubated in darkness at 25°C. Germinated acorn radicles from 10-day-old cork oak seedlings with no sign of shoot apical meristem or lateral roots and ranging from 4 to 8 cm in length were used for the root assay.

Phytophthora cinnamomi PA-45, isolated in the Algarve region from soil associated with declining cork oak stands (Horta et al. 2008), was highly virulent on cork oak seedlings, causing extended necrotic lesions on root tissues 48 h after inoculation (Horta et al. 2010). To enhance the potential of infection, cultures of PA-45 were induced to produce zoospores (Chen and Zentmyer 1970). Briefly, 3-day-old cultures of *P. cinnamomi* PA-45 growing on V8 agar (2% autoclaved V8 vegetable juice, Campbell Foods Belgium S.A., Puurs, Belgium, 1.6% Bacto Agar) at 24°C were used as inoculum for the production of young sensitive mycelium. Mycelium plugs (10 mm^2) from the actively growing cultures were transferred to sterilized test tubes containing 20 ml autoclaved and clarified V8 broth medium (2%). Transferred mycelium was incubated for 1 day at 24°C in darkness. Sporangial production was induced by washing young and sensitive mycelial mats three times with autoclaved mineral salt solution (MSS, 10 mM calcium nitrate, 5 mM potassium nitrate and 4 mM magnesium sulphate) amended with filter-sterilized (0.2 μm) chelated iron (Fe-EDTA, ethylenediaminetetraacetic acid ferric sodium salt; Sigma-Aldrich, Steinheim, Germany). Finally, mycelial mats were incubated in 20 ml sterile MSS amended with Fe-EDTA for 1 day at 24°C under fluorescent light suspended 40 cm above (108 μmol m^{-2} s^{-1} cool white). Zoospore release was observed under light microscopy using a Leica DM LB microscope (Wetzlar, Germany) with 100× magnification. Zoospore concentration was measured with a counting chamber (Fuchs Rosenthal; Hausser Scientific, Horsham, PA, USA) in aliquots of 100 μl randomly sampled from MSS suspension (n = 5). The final pathogen suspension for the root assay consisted of an average of 10^5 zoospores in 20 ml autoclaved MSS with sporangia-derived mycelia. For the mycelium assay, the emerged zoospores were washed once with autoclaved MSS and the sporangia-derived mycelia exposed to cork oak root exudates as described below.

2.2 Experimental design

The cork oak root assay consisted of seedlings inoculated with *P. cinnamomi* and mock-inoculated seedlings ('biotic' factor, n = 2) sampled at 2, 8, 16 and 24 h post-inoculation (hpi, 'temporal' factor, n = 4) as independent variables. Five roots were used individually for each treatment as biological replicates. Cork oak acorns with germinated radicles ranging from 4 to 8 cm in length were mounted on test tubes, allowing radicles, but not the acorns, to be immersed into the zoospore suspension. Roots were carefully mounted to avoid direct contact with precipitated mycelial mats; hence, host inoculation was restricted to zoospore infection. Cork oak seedlings were incubated at 24°C in darkness and harvested at 2, 8, 16 and 24 hpi. The distal root ends were cut approximately 3 cm from the tips, rapidly snap-frozen in liquid nitrogen and stored at −80°C until further analysis by FT-IR.

For the mycelium assay, mycelium of *P. cinnamomi* exposed to cork oak root exudates and autoclaved MSS (mock-exposed, 'biotic' factor, n = 2) was sampled at 8, 16 and 24 h post-exposure (hpe, 'temporal' factor, n = 3) as independent variables. Mycelium samples at 2 hpe were also collected; however, the material was insufficient for FT-IR measurement, and thus, this time point was removed from the mycelium assay. Four mycelial mats were used individually for each treatment as biological replicates. Cork oak root exudates were collected from germinated seedlings with 6–9 true leaves and radicles ranging from 8 to 10 cm long (n = 20) incubated in 900 ml autoclaved MSS for 1 day at 24°C on the laboratory workbench (Lanoue et al. 2010). The hydroponic solution was filter-sterilized (0.2 μm) twice to remove potential microbial contamination and plant cells. Then, the sporangia-derived mycelial mats were incubated in either 20 ml freshly filter-sterilized cork oak root exudates or 20 ml autoclaved MSS for the mock-exposed treatment at 24°C in darkness. At the

predetermined sampling times (8, 16 and 24 hpe), mycelial mats were carefully detached from the cultivated agar medium with a sterile glass Pasteur pipette and gently squeezed to remove excess of MSS solution. Finally, mycelial mats were frozen in liquid nitrogen and stored at $-80°C$.

2.3 Metabolic profiling with FT-IR spectroscopy

Prior to FT-IR analysis, biological samples (roots and mycelium) were ground in liquid nitrogen with a mortar and pestle. To prevent transformation of metabolites and FT-IR absorbance of O–H molecular vibration derived from water molecules, root tissues (c.a. 5 g) and mycelial mats (c.a. 50 mg) were lyophilized for 16 and 32 h, respectively (Micro Modulyo Freeze Dryer; Edwards, Crawley, UK). Lyophilized samples were blended with KBr powder (Aldrich Chemical Co., Milwaukee, WI, USA) in a 1 : 3 ratio and vacuum-pressed (10 t) to obtain a translucent pellet. Pellets were scanned in the middle-infrared spectrum (4000–400 cm^{-1}) with average over 125 scans at a resolution of four wavenumbers (cm^{-1}) in the FT-IR Spectrophotometer (TENSOR 27 series – Bruker Optik GmbH, Ettlingen, Germany). A total of four individual FT-IR spectra were generated for each biological sample: two translucent pellets were prepared for each biological sample as preparation replicates and the FT-IR spectra of these pellets were measured twice as technical replicates. The transmittance FT-IR spectra generated were preprocessed using OPUS software (Bruker GmbH, v 5.5). Each spectrum was corrected with straight line to compensate atmospheric CO_2 peaks (2400–2275 cm^{-1}), subjected to baseline correction using the rubber band algorithm with 64 points correction, smoothed with Savitzky–Golay filter (9 points) and finally vector-normalized (Lecellier et al. 2014). Briefly, first the average *y*-value of the spectrum in the region of concern was calculated. This average *y*-value was subtracted from the spectrum, resulting in a spectrum centred around $y = 0$. This respective spectrum was divided by the square root of the sum of *y*-value squares. Homogeneous FT-IR spectra from technical replicates were averaged by arithmetic mean and used as representatives of the biological sample. The whole profile spectrum with 1866 reading positions (wavenumbers cm^{-1}) was exported as tab-delimited file and used for recognition of patterns across treatments. In addition, the FT-IR band positions (wavenumber cm^{-1}) were measured according to the centre of weight using a 0.2% sensitivity parameter from the peak-picking function (OPUS software) and exported as described above.

2.4 Data and statistical analyses

The whole FT-IR spectrum data from root and mycelium samples were kept separated, and each was imported into R project (R Core Team 2013). The FT-IR 'wavenumbers' (n = 1866) and transmittance values (i.e. intensity) were treated as independent and dependent variables, respectively (Wehrens 2011).

To determine significance between means of 'biotic' levels, Student's t-tests were applied to each wavenumber for each 'temporal' level. Pattern recognition was carried out with principal component analysis (PCA) by computing a singular value decomposition of the data set with function prcomp from R (Logan 2010). For this process, the original matrix was vector-normalized (along columns) by scaling the data to achieve a mean of 0 and a standard deviation of 1 (R Core Team 2013). A density plot was used to confirm normalization of the data. The ordination diagram was generated with the assigned object scores relative to each principal component (PC). For both biological systems, the two-first PCs were used to identify the levels of significance from 'biotic' and 'temporal' variables by ANOVA (Logan 2010).

To access metabolic patterns across 'temporal' levels, the transmittance value of assigned bands was transformed to absorbance value ($A = \log_{10} 1/T$). The FT-IR band matrix was vector-normalized by the min–max normalization module (Jain et al. 2005) and metabolic patterns computed by Pearson's correlation coefficient using R (R Core Team 2013) after subtracting each FT-IR absorbance band of inoculated and exposed samples from those of mock-inoculated and mock-exposed in a given time, respectively. This process reduces the effect of natural metabolic evolution and provides evidence of the effect of the interaction. Pattern correlation was illustrated by a dendrogram of FT-IR bands using the function heatmap.2 from the gplots library (R Core Team 2013).

When assumptions of homogeneity of variance and normality were violated, Welch's test and the Kruskal–Wallis test, combined with Nemenyi-rank multiple comparison (1000 permutations), were applied, respectively (Logan 2010). A treatment was considered to differ significantly when an alpha level of <0.05 was observed.

3 Results

3.1 FT-IR spectral patterns from cork oak roots inoculated with *P. cinnamomi*

The FT-IR spectra showed typical complex patterns with many overlapping bands observed at lower (1500–400 cm^{-1}) and higher frequency regions (3700–2400 cm^{-1}, Fig. 1). The overall FT-IR root spectrum was characterized by a total of 18 bands (i.e. Q1–Q18) grouped according to assigned functional groups and putative biochemical groups (Table 1). Within each sampling time, FT-IR spectra from inoculated roots revealed major differences at 2, 8 and 24 hpi when compared to mock-inoculated roots (Fig. 1). At 2 hpi, inoculated plants had significantly enhanced levels of bands Q1 (3481–3271 cm^{-1}) and Q15/Q16 (765–711 cm^{-1}) and significantly reduced levels for bands Q2 (3122–2983 and 2952–2545 cm^{-1}) and Q3 (1780–1739 cm^{-1}) when compared to mock-inoculated plants (Fig. 1a). These differences were further extended (seven regions) at 8 hpi with the intensity of bands Q1 (3489–3207 cm^{-1}), Q12/Q13 (948–833 cm^{-1}) and region 2468–1793 (wavenumber cm^{-1}) significantly enhanced in inoculated plants, whereas several bands were significantly reduced Q2 (3141–2850 cm^{-1}), Q3 (1766–1697 cm^{-1}), Q7 (1377–1367 cm^{-1}) and region 3697–3587
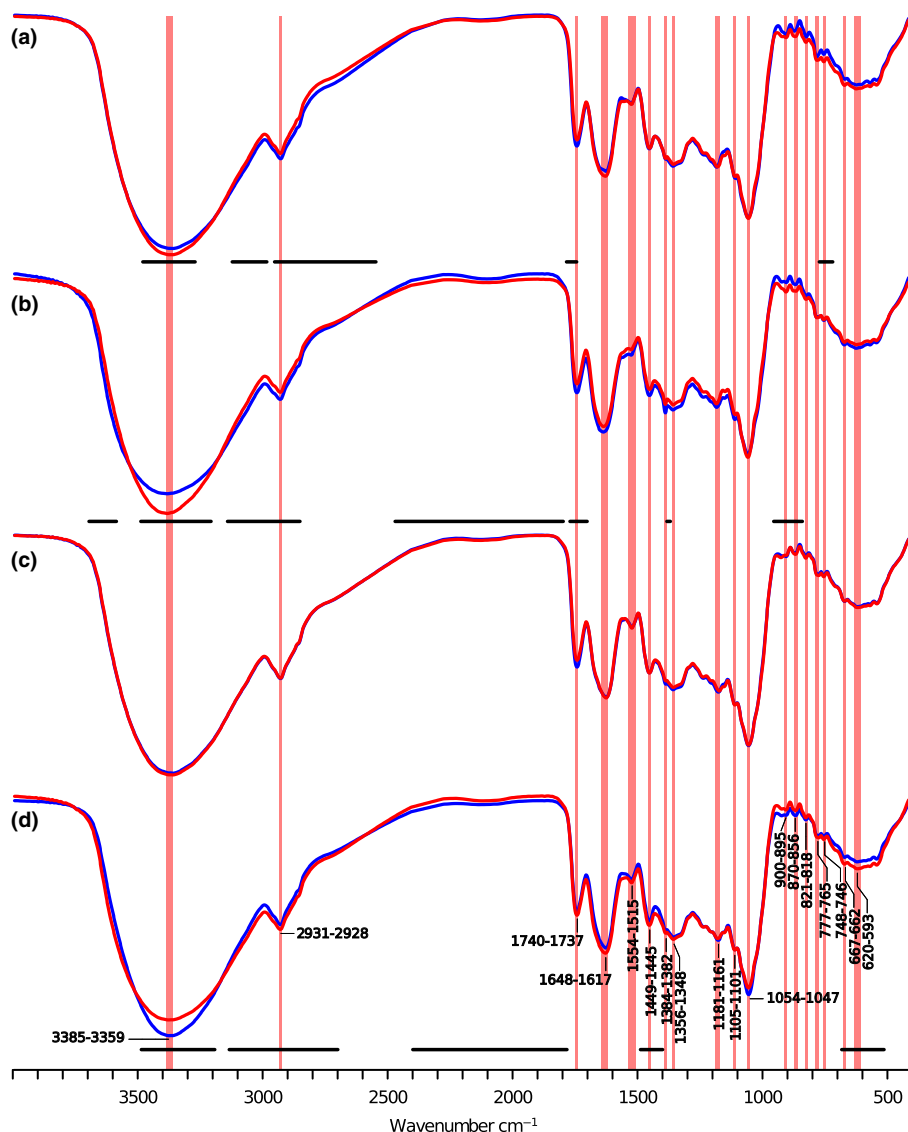
Fig. 1. Fourier transform-infrared (FT-IR) spectra of cork oak roots inoculated with *P. cinnamomi* (red line) and mock-inoculated (blue line). FT-IR spectra are shown as transmittance values of arithmetic means from five replicate root samples 2, 8, 16 and 24 h post-inoculation (panels a, b, c and d, respectively). The FT-IR spectra in each panel are drawn to have identical vertical scales (i.e. same intensity for all panels). Wavenumber regions with significant levels of difference are shown in bold black lines below each set of FT-IR spectra. On panel d, the infrared wavenumbers (cm^{-1}) of selected bands (Q1–Q18) are also shown. FT-IR bands are shown in the range from where all cork oak samples were observed.

(wavenumber cm^{-1}) when compared to mock-inoculated plants (Fig. 1b). No significant difference ($p > 0.05$) was observed between FT-IR spectra derived from inoculated and mock-inoculated plants at 16 hpi (Fig. 1c). At 24 hpi, the intensity of band Q1 (3487–3192 cm^{-1}) and region 2397–1778 (cm^{-1}) was significantly reduced in inoculated plants, whereas bands Q2 (3134–2698 cm^{-1}), Q6 (1483–1394 cm^{-1}) and Q17/Q18 (675–505 cm^{-1}) were significantly enhanced when compared to mock-inoculated plants (Fig. 1d).

The contribution of each independent variable 'wavenumbers' to discriminate 'biotic' and 'temporal' factors was further explored with PCA. The ordination diagram with the object scores was generated from the two-first PCs and accounted for 75.3% of the total variability (Fig. 2). The largest PC (PC1) mainly distinguished samples from 8 (inoculated and mock-inoculated plants) and 24 hpi (mock-inoculated plants) from roots sampled at 2 and 16 hpi. These samples were scattered on the positive score gradient of PC1 and were largely characterized by the significant decrease in absorbance at the regions associated with bands Q2 (2981–2648 cm^{-1}) and Q6 (1461–1446 cm^{-1}). Mock-inoculated samples from 8 hpi were significantly different ($p < 0.01$) from all other sampling times, while inoculated samples from 8 hpi differed significantly from those at 2 and 16 hpi. Mock-inoculated samples from 2 and 16 hpi were found exclusively on the negative score gradient of PC1 and were mainly characterized by absorbance at 3502–3452 (wavenumber cm^{-1}). Samples from mock-inoculated plants at 8 and 24 hpi plotted, respectively, in the upper and lower score gradient of PC2 and were

Table 1. Tentative assignment of infrared bands to molecular vibrations of functional groups and biochemical compounds (Coates 2000; Chalmers and Griffiths 2002; Stuart 2004).

Spectral region, cm⁻¹	Cork oak roots Band[1]	Cork oak roots Wave number, cm⁻¹	Phytophthora cinnamomi mycelia Wave number, cm⁻¹	Phytophthora cinnamomi mycelia Band[1]	Vibrational modes	Functional groups	Biochemical compounds
>3000	Q1_sb	3385–3359	3420–3385	P1_sb	ν O–H; ν N–H; ν C–H	Alcohols; carboxylic acids; amines and amides; unsaturated and aromatic hydrocarbons	Carbohydrates and glycoconjugates
3000–2800 (fatty acids)	Q2_m	2931–2928	2925–2922	P2_m	ν_{as} CH₂, CH₃	Saturated hydrocarbons	Lipids
			2858–2855	P3_w	ν_s CH₂, CH₃		
1750–1650	Q3_m	1740–1737			ν C=O	Carbonyl of aldehydes, ketones, esters and carboxylic acids	Fatty acids, aliphatic and aromatic carbonyl-containing compounds
1650–1500 (protein)	Q4_sm	1648–1617	1653–1646	P4_m	ν C=C; ν C=O; δ_s NH₂	Unsaturated and aromatic hydrocarbons; amides (Amide I and Amide II); amines	Proteins; peptidoglycans
	Q5_m	1554–1515	1553–1543	P5_w	ν C–N; δ NH		
1500–1250 (fatty acids)	Q6_m	1449–1445	1464–1459	P6_wm	ρ CH₃; δ_s CH₂; δ_s CH₃; ω CH₂	Saturated and unsaturated hydrocarbons; carboxylic acids; carboxylic acid salts; alcohols and phenols; esters; amines;	Glycoconjugates; proteins; fatty acids; amino acids; phospholipids; nucleic acids
	Q7_m	1384–1382	1384–1383	P7_s	τ CH₂; δ C=C–H; δ O–H; δ C–O–H		
	Q8_m	1356–1348			δ N–H; ν C–N;		
			1250–1247	P8_w	ν C–O; ν_s COO⁻; ν P=O	amides (Amide III); phosphate esters	
1200–900 (cellulosic domain)	Q9_m	1181–1161	1203–1200	P9_w	ν C–O; ν C–C; δ C=C–H; ν C–N;	Alcohols and phenols; saturated and aromatic; hydrocarbons; ethers; amines; esters; phosphate esters	Phospholipids; nucleic acids; polysaccharides; phenolic compounds
	Q10_m	1105–1101	1158–1157	P10_m	ν P=O; ν_{as} P–O–C		
			1110–1107	P11_m			
	Q11_s	1054–1047	1077–1074	P12_s			
			1045–1043	P13_s			
<900	Q12_w	900–895	895–891	P14_w	δ_{oop} C–H; δ_{oop} O–H;	Hydrocarbons; carboxylic acids; peroxides; hydroperoxides; alcohols; phosphate esters; amines; amides	Cell wall glycoconjugates; lipid peroxides; aromatic-containing compounds; phospholipids; nucleic acids; lipids; nitrogen-containing compounds; polysaccharides
	Q13_w	870–856			ν O–O; ν O–OH;		
	Q14_w	821–818	830–824	P15_w	ν_s P–O–C; ρ CH₂;		
	Q15_w	777–765			ω N–H; τ N–H		
	Q16_w	748–746					
	Q17_w	667–662	669–656	P16_w			
	Q18_w	620–593	606–598	P17_w			

ν, stretch (s – symmetric; as – asymmetric); δ, in-plane bending; δ_{oop}, out-of-plane bending; δ_{sc}, scissoring; ρ, rocking; ω, wagging; τ, twisting. [1]Bands from the FT-IR spectra of cork oak roots and *P. cinnamomi* mycelia shown in Figs 1 and 4, respectively. Relative intensities: sb – strong and broad; s, strong; m, moderate; w, weak.
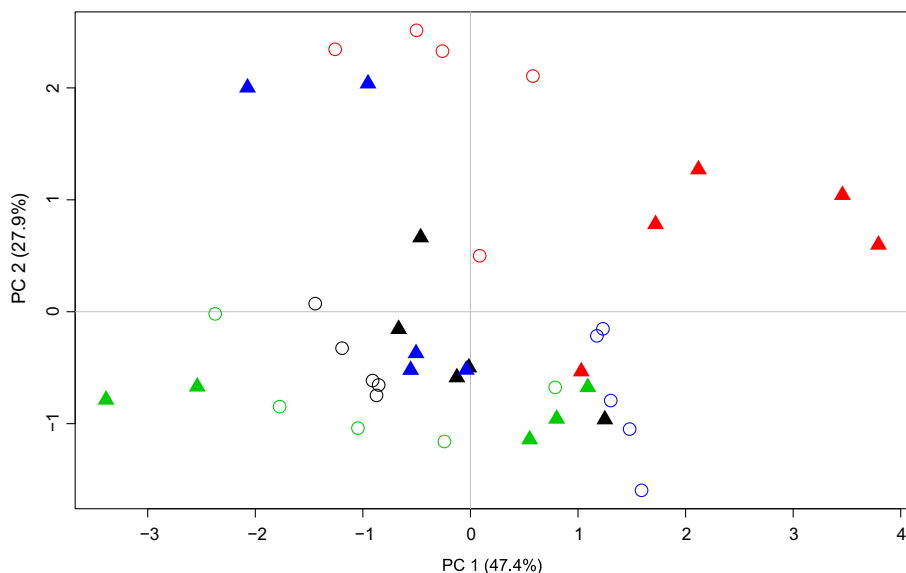
Fig. 2. Ordination diagram generated by principal component analysis (PCA) on the basis of Fourier transform-infrared (FT-IR) spectra collected from inoculated (triangle) and mock-inoculated (circle) cork oak roots. Samples collected at 2, 8, 16 and 24 h post-inoculation are shown in black, red, green and blue signs, respectively. The percentages indicate the proportions of variation explained by the first and second ordination axes.

significantly different (p < 0.001) when compared to inoculated samples (Fig. 2). Four replicates from mock-inoculated samples at 8 h were mainly distinguished by the FT-IR spectrum at 2403–2281 (wavenumber cm^{-1}), whereas mock-inoculated samples at 24 hpi were mainly characterized by reduced absorbance at 3654–3608 (cm^{-1}) and associated with the band Q18 (646–507 cm^{-1}).

Pattern correlation analysis revealed three conspicuous clusters of FT-IR patterns from *Q. suber* assigned bands that were significantly correlated ($r > 0.53$; p < 0.001) (Figure S1). FT-IR bands Q1, Q11, Q12 and Q13 were positively correlated ($r > 0.7$; p < 0.001) and showed a reduction in the pattern of absorbance from 8 to 24 hpi (Fig. 3; Table S1). FT-IR
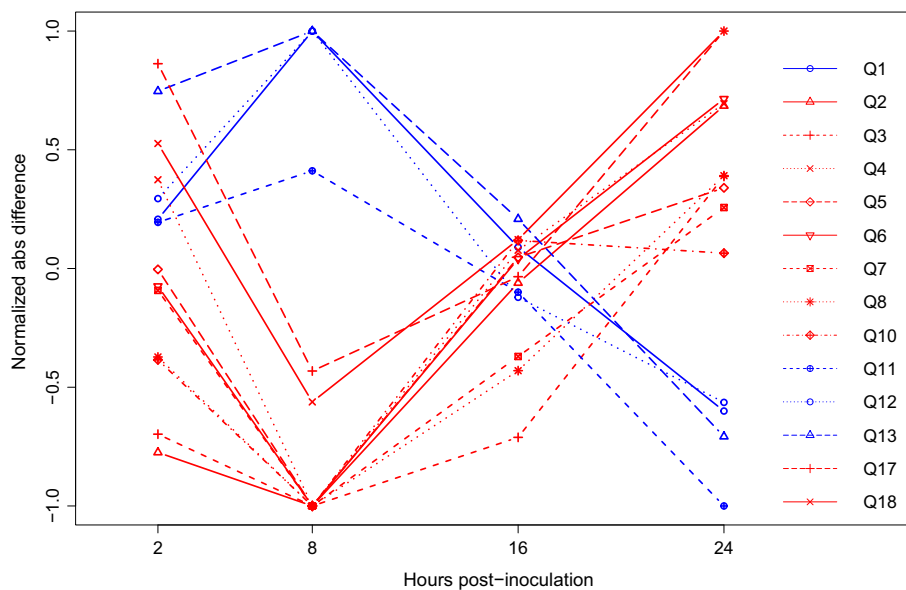

Fig. 3. Patterns of metabolic changes from *Quercus suber* Fourier transform-infrared (FT-IR) bands with time. Two distinct metabolic patterns of *Q. suber* seedlings when challenged by *Phytophthora cinnamomi* are shown. Metabolites related to carbohydrate groups are represented by blue (bands Q1, Q11, Q12 and Q13) lines, and those related to lipid and protein groups are represented by red (bands Q2–Q10, Q17 and Q18) lines. A positive value on the *y*-axis indicates higher concentrations of metabolic groups (FT-IR bands) in the seedlings of *Q. suber* inoculated with *P. cinnamomi*, whereas negative values indicate higher concentrations of metabolic groups in the seedlings of *Q. suber* that were mock-inoculated.

bands Q2, Q3, Q4, Q5, Q6, Q7, Q8, Q10, Q17 and Q18 were also positively correlated ($r > 0.53$; $p < 0.001$), displaying a second distinct configuration with a reduction in the pattern of absorbance at 8 hpi followed by an increase in succeeding hours (Fig. 3). Independent of the FT-IR pattern group, these bands revealed a conspicuous convergence in the pattern of absorbance at 16 hpi between inoculated and mock-inoculated plants, followed by the inverse pattern at 24 hpi when compared to samples collected at 8 hpi (Fig. 3). The pattern of the remaining FT-IR bands Q9, Q15 and Q16 was also positive correlated ($r > 0.76$; $p < 0.001$; Table S1).

3.2 FT-IR spectral patterns of *P. cinnamomi* mycelium exposed to cork oak root exudates

Mycelium of *P. cinnamomi* collected at 8, 16 and 24 hpe to cork oak root exudates or MSS (control treatment) displayed complex metabolic profiles with many overlapping bands at the lower frequency of the FT-IR spectrum (1500–400 cm^{-1}, Fig. 4). FT-IR spectra from mycelial samples were characterized by 17 bands (P1–P17, Table 1), grouped according to assigned functional groups and putative biochemical groups (Table 1). All FT-IR spectra of *P. cinnamomi* mycelium had an almost undetectable weak shoulder band of carbonyl (~1740 cm^{-1}). Within each sampling time, specific regions of the FT-IR spectra from mycelium exposed to cork oak root exudates differed significantly when compared to spectra from mock-exposed mycelium (Fig. 4). At 8 hpe, the intensity of band P7 (1404–1348 cm^{-1}) and region 3328–3240 (wavenumber cm^{-1}) was significantly reduced and enhanced in mycelium samples exposed to root exudates when compared to mock-exposed mycelium, respectively (Fig. 4a). At 16 hpe, the intensity of bands P2, P3 (2974–2842 cm^{-1}), P4 (1760–1652 cm^{-1}), P5 (1571–1508 cm^{-1}), P8/P9 (1303–1195 cm^{-1}) and region 1018–968 (cm^{-1}) was significantly reduced in mycelium samples exposed to root exudates (Fig. 4b). At 24 hpe, the intensity of bands P1 (3492–3317 cm^{-1}), P14/P15 (956–788 cm^{-1}) and region 2594–1755 (cm^{-1}) was significantly reduced in mycelium samples exposed to cork oak root exudates, whereas regions 3251–2974 and 1151–1114 (cm^{-1}) and band P4 (1679–1560 cm^{-1}) were significantly enhanced when compared to mock-exposed mycelium (Fig. 4c).
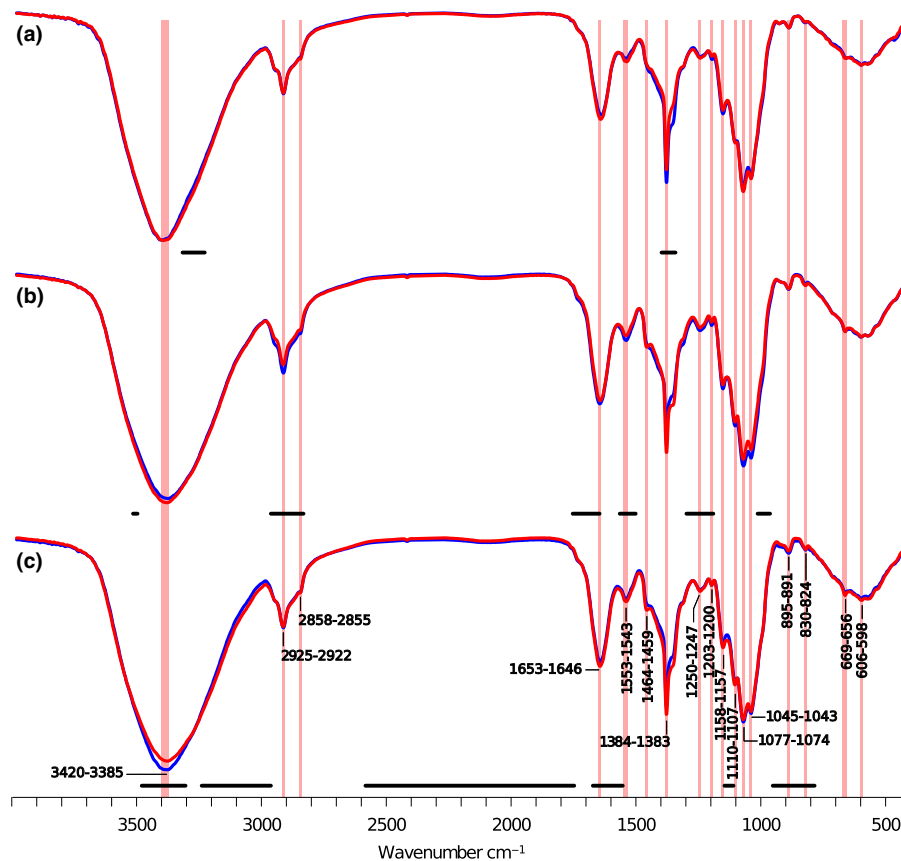

Fig. 4. Fourier transform-infrared (FT-IR) spectra of mycelium from *P. cinnamomi* exposed to cork oak root exudates (red line) or control (blue line). FT-IR spectra are shown as transmittance values of the arithmetic mean from four mycelial replicates 8 (panel a), 16 (b) and 24 h post-exposure (c). FT-IR spectra in each panel are prepared with identical vertical scales (i.e. same intensity for all panels). Wavenumber regions with significant differences are shown in bold black lines below each set of FT-IR spectra. Panel (c) also shows the infrared wavenumbers (cm^{-1}) of selected bands (P1–P17). FT-IR bands are shown in the range from where all mycelium samples were observed.
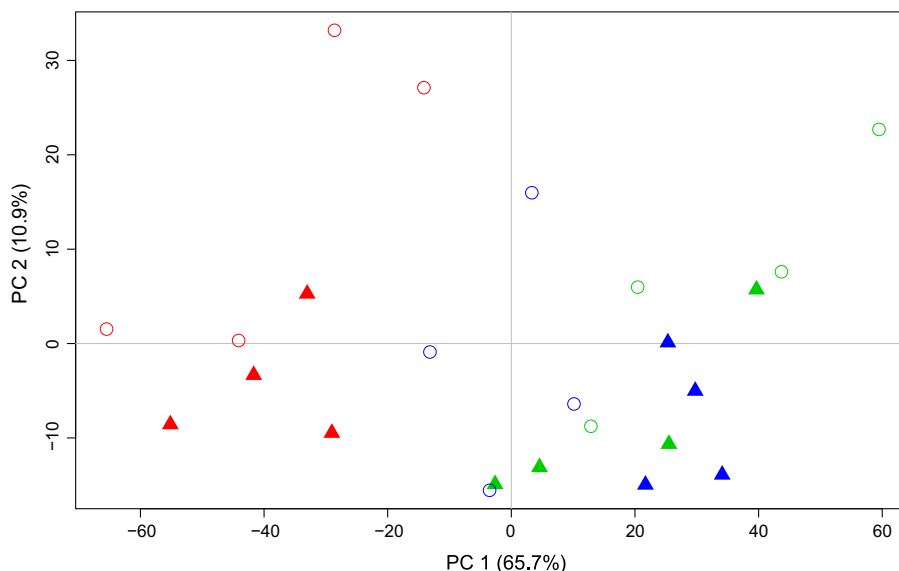
Fig. 5. Ordination diagram generated by principal component analysis (PCA) on the basis of Fourier transform-infrared (FT-IR) spectra collected from mycelium exposed to cork oak root exudates (triangle) and mock-exposed (circle). Samples collected at 8, 16 and 24 h post-inoculation are shown in red, green and blue signs, respectively. The percentages indicate the proportions of variation explained by the first and second ordination axes.

The ordination diagram of mycelium samples was generated from the PC1 and PC2 PCs and accounted for 76.6% of the total data variability (Fig. 5). The large variability of the score plot was explained by PC1 (65.7%), which distinguished scores mainly by 'temporal' factor. Samples from 8 h were exclusively plotted on the negative score gradient of PC1 and were significantly different ($p < 0.01$) from those of 16 and 24 hpe found on the central and positive score gradient of PC1. Mycelium samples from 8 h were mainly characterized by reduced absorbance at regions of bands P2 (3171–2976 cm^{-1}), P4 (1709–1655 cm^{-1}) and P5 (1582–1558 cm^{-1}), while samples from 16 and 24 hpe were largely characterized by reduced absorbance at regions associated with bands P1 (3489–3352 cm^{-1}), P14 (872–841 cm^{-1}) and region 2596–1794 (cm^{-1}). At 24 h, all samples from mycelium exposed to root exudates were closer, but distinct from samples of control mycelium, mostly scattered on the left-hand side of the plot (Fig. 5). Although PC2 showed reduced variability (only 10.9%), samples from mycelium exposed to root exudates at 8 and 16 hpe mainly plotted at the negative score gradient of PC2 and were characterized by reduced absorbance of band P9 (1204–1196 cm^{-1}) and region 980–974 (wavenumbers cm^{-1}), while mycelium samples exposed to MSS were mainly scattered on the positive score gradient of PC2 and were characterized by enhanced absorbance at regions 3310–3283 and 2775–2770 (cm^{-1}; Fig. 5).

Correlation analysis revealed six conspicuous patterns that significantly correlated within clusters of *P. cinnamomi* FT-IR assigned bands ($r > 0.93$; $p < 0.001$) (Figure S2). FT-IR bands P2, P6, P9 and P16 were positively correlated ($r > 0.98$; $p < 0.001$) and showed a constant increase in the pattern of absorbance with sampling time (Fig. 6; Table S2). FT-IR bands P3, P4, P5, P8 and P11 were positively correlated ($r > 0.93$; $p < 0.001$) and showed distinct reductions in pattern of absorbance at 8 hpe followed by an increase at 24 hpe (Fig. 6). The four remaining patterns were observed as pairs of FT-IR bands P1/P14, P7/P15, P10/P17 and P12/P13, each of which was also positively correlated ($r > 0.95$; $p < 0.001$) and showed a distinct pattern of absorbance (Fig. 6).

4 Discussion

In contrast to other metabolic profiling techniques, for example GC–MS and LC–MS, which involve separation of molecules by chromatography, FT-IR spectroscopy detects antisymmetric vibration of polar molecules and thus generates a 'holistic' overview of major functional groups retrieved from the biological system under investigation. Hence, the rapid screening capacity and ability to detect unforeseen metabolic alterations in biological systems makes FT-IR spectroscopy a suitable technique to be used prior to any targeted metabolite analysis (Chalmers and Griffiths 2002). Nevertheless, the use of FT-IR spectroscopy in woody plant–pathogen interactions is scarce and even more singular when the considering temporal effects (Martín et al. 2005; Allwood et al. 2006; Cameron et al. 2006; Martin et al. 2007, 2008; Conrad et al. 2014; Vivas et al. 2014). So, to our knowledge, this article is the first to describe temporal changes in the metabolic patterns of early interaction between cork oak roots and *P. cinnamomi* by FT-IR spectroscopy.

At a first glance, the hyperspectral data generated by the FT-IR technique revealed high complexity. Therefore, we relied on statistical analyses to discriminate FT-IR regions for each investigated variable (i.e. 'biotic' and 'temporal') and to correlate changes in metabolic patterns from assigned bands along the 'temporal' variable. It is clear, even at the earlier
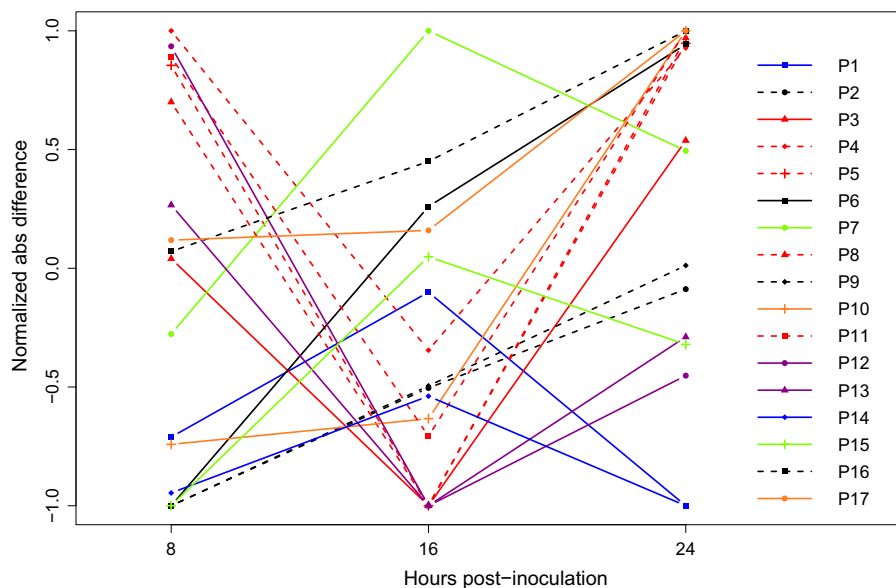
Fig. 6. Patterns of metabolic changes in *Phytophthora cinnamomi* Fourier transform-infrared (FT-IR) bands with time. Six distinct metabolic patterns of *P. cinnamomi* mycelium when exposed to *Quercus suber* root exudates are shown. Positive values on the *y*-axis indicate higher concentrations of metabolic groups (FT-IR bands) in the mycelium of *P. cinnamomi* exposed to *Q. suber* root exudates, whereas negative values indicate higher concentrations of metabolic groups in the mycelium of *P. cinnamomi* that was mock-exposed.

sampling time, that cork oak plants showed abrupt alterations to the metabolites when inoculated with *P. cinnamomi*, suggesting rapid adjustments in the host metabolic profile. Also, the contribution of *P. cinnamomi* metabolites to the overall metabolic pattern observed with time cannot be excluded. Colonization of susceptible hosts by *Phytophthora* spp. results in a significant increase in pathogen biomass within days of inoculation (Kamoun et al. 1998; Asai et al. 2010).

In this work, the FT-IR analysis of *Q. suber* plants inoculated with *P. cinnamomi* revealed two very distinct patterns that contrasted in terms of concentration of functional groups with time. Carbohydrate (band Q1) and cell wall glycoconjugate (bands Q11, Q12 and Q13) groups were enhanced, as early as 2 h after inoculation, until 8 hpi, whereas lipid (bands Q2, Q6, Q7 and Q8), carbonyl (band Q3), protein (bands Q4 and Q5) and cell wall glycoconjugate (bands Q10, Q17 and Q18) groups were drastically reduced at the same time. Photoassimilates are synthesized to supply essential energy for cell growth and development. Upon invasion, *P. cinnamomi* probably disrupted this state of homeostasis. However, it was not clear whether the increment in the host carbohydrates was due to the pathogen reprogramming host metabolism to support pathogenesis (Hückelhoven 2007; Martin and Kamoun 2012) or was a restructuring of host metabolism to counter pathogen invasion. For instance, cell wall-associated defence responses might include papillae apposition. Addition of glyco-conjugate groups at region of bands Q11 and Q12 (± 1050 and ± 900 cm^{-1}, respectively) has been associated with the apposition of xyloglucans (Morris et al. 2003). Xyloglucan, a hemicellulosic polysaccharide important in the formation of primary wood cell walls, is also one of the constituents of papillae during cell wall apposition upon oomycete invasion (Enkerli et al. 1997; Underwood 2012; Oßwald et al. 2014).

The reduction in the level of lipid groups was also detected in plants of *Brachypodium distachyon* when inoculated with the fungus *Magnaporthe grisea* (Allwood et al. 2006). A central event in plant resistance during progress of pathogen invasion is the activation of ROS generation, a reaction also known as the 'oxidative burst' (De Jong et al. 2004; Testerink and Munnik 2005). Increases in ROS lead to the oxidative degradation of lignin, cellulose and lipid groups, thus affecting membrane permeability and consequently inducing apoptosis (Spiteller 2003; Torres et al. 2006). Although the concentration of ROS was not directly quantified in this work, cork oak plants inoculated with *P. cinnamomi* had extensive root necrosis, an indirect sign of the 'oxidative burst' (Horta et al. 2010; Medeira et al. 2012).

After the initial host disturbance, no differences between the FT-IR spectra from inoculated and mock-inoculated plants at 16 hpi were found. This result might be explained by the reorganization of the host cell metabolites observed after being subjected to biotic (Vega-Sanchez et al. 2005; Kelley et al. 2010) and abiotic stresses (Kim et al. 2007). A new metabolic pattern emerged at 24 hpi with the accumulation of lipid, protein and aromatic-containing groups, and a reduction in the level of carbohydrate and glycoconjugate groups. In elm trees (*Ulmus minor*), the reduction in carbohydrate groups was inversely correlated to the increasing lignification in the xylem several days after inoculation with *Ophiostoma novo-ulmi*, suggesting activation of induced host defence responses (Martín et al. 2005). The increase in the phospholipid phosphatidic acid (PA), observed in FT-IR region 1350–1250 cm^{-1} (band Q8), has been associated with resistance of *B. distachyon* when challenged by the fungus *M. grisea* (Allwood et al. 2006). PA is a signalling molecule involved in various cell processes, including defence against biotic challenges, that leads to the oxidative burst in plants (De Jong et al. 2004; Allwood et al. 2006; Wang et al. 2006). ROS will also activate the pentose phosphate pathway, providing pentose intermediates for the

production of aromatic compounds, such as phenolic compounds and their derivatives that might contribute to the cell wall reinforcement via apposition of suberin, lignin and callose (Pugin et al. 1997). These are major cell wall components containing lipid polyester and phenolic moieties that impart resistance to pathogens (Pollard et al. 2008; Vanholme et al. 2010). Thus, the accumulation of lipid groups might be related reinforcement of the cell wall physical barrier (Martín et al. 2005). Based on the molecular mechanism model proposed by Coelho et al. (2011), *Q. suber* will also upregulate phenylpropanoid metabolism upon recognition of *P. cinnamomi* effector molecules, leading to a cascade of events that culminates in cell wall reinforcement. In addition, suberin has been positively correlated with resistance to *Phytophthora* invasion (Thomas et al. 2007) and cork oak is notorious for suberin synthesis to protect it against abiotic and biotic stresses (Cordeiro et al. 1998). Inoculation of *Pinus pinaster* with *Fusarium circinatum* induced the accumulation of methylesterified pectin polysaccharides and the reduction of non-esterified pectin polysaccharides (Vivas et al. 2014). Similar carbohydrate patterns were observed in the samples analysed in the present work and support the use of methylesterified pectins (band Q10) as biomarkers for the identification of resistant individuals after biotic stress (Taoutaou et al. 2012; Vivas et al. 2014).

Mycelium of *P. cinnamomi* also showed distinct metabolic patterns when exposed to *Q. suber* root exudates. A total of six distinct patterns were identified, suggesting that mycelium of *P. cinnamomi* rearranged its nutritional metabolism in the presence of water-soluble root exudates. Also one might assume natural adjustments of the metabolic profile during nutrient depletion (Chen and Zentmyer 1970). FT-IR analysis revealed that bands putatively assigned to lipid (P3 and P8), protein (P4 and P5) and cell wall (P11) groups were detected in higher proportions in mycelium exposed to root exudates at 8 and 24 hpe but not at 16 hpe. It is not clear whether the increment in protein content is related to the synthesis of effector proteins. However, synthesis of effector proteins and elevated activities of plant cell wall degrading enzymes such as pectinases have been observed when *Phytophthora* spp., including *P. cinnamomi* PA-45, infect host plants, including *Q. suber* (Horta et al. 2008; Martin and Kamoun 2012). Accumulation of lipid (band P2 and P6) groups in mycelium exposed to root exudates was also observed with time. In addition to effector proteins, which are characterized as narrow host range effectors, there are others, such as glucans and fatty acids, which are synthesized by broad host range pathogens like *P. cinnamomi* (Tyler 2002). Unfortunately, FT-IR does not have sufficient resolution to identify single molecules. Nevertheless, our data corroborate previous results, which showed the capacity of *Phytophthora* to detect and respond to root exudates of woody plants, including from *Quercus* (Kozlowski 1997; Cots and Tuset 2002).

It is well known that the outcome of plant–pathogen interactions is a balance between pathogen invasion machineries and host defence responses (Jones and Dangl 2006). The work reported here has shown that the interaction between cork oak plants and *P. cinnamomi* is highly complex, with both biological systems accommodating their metabolic profiling within hours of the initiation of the interaction. The two distinct metabolic patterns observed in the host with time after inoculation could also be an adaptation of the pathogen to acquire nutrients during the transition from a biotrophic to a necrotrophic life strategy (Qutob et al. 2002). The shift in the host metabolic pattern of carbohydrate and lipid groups suggests a remarkable and dynamic host response to *P. cinnamomi* invasion and that *Q. suber* seedlings were resistant to pathogen invasion. On the other hand, alterations in the pathogen metabolic pattern of carbohydrate, lipid and protein groups were remarkable in the presence of cork oak root exudates. Overall, these results demonstrated that the metabolic patterns of both biological systems are quite dynamic with time of interaction and that this effect should be taken into account when discriminating metabolic patterns from biological systems, especially during the early hours of plant–pathogen interactions.

Acknowledgements

References

Allwood, J. W.; Ellis, D. I.; Heald, J. K.; Goodacre, R.; Mur, L. A. J., 2006: Metabolomic approaches reveal that phosphatidic and phosphatidyl glycerol phospholipids are major discriminatory non-polar metabolites in responses by *Brachypodium distachyon* to challenge by *Magnaporthe grisea*. Plant J. **46**, 351–368.

Asai, S.; Mase, K.; Yoshioka, H., 2010: A key enzyme for flavin synthesis is required for nitric oxide and reactive oxygen species production in disease resistance. Plant J. **62**, 911–924.

Brasier, C. M., 2008: The biosecurity threat to the UK and global environment from international trade in plants. Plant. Pathol. **57**, 792–808.

Brasier, C. M.; Robredo, F.; Ferraz, J. F. P., 1993: Evidence for *Phytophthora cinnamomi* involvement in Iberian oak decline. Plant. Pathol. **42**, 140–145.

Brereton, R. G., 2009: Chemometrics for Pattern Recognition. Chichester: Wiley-Blackwell, pp. 522.

Bugalho, M. N.; Caldeira, M. C.; Pereira, J. S.; Aronson, J.; Pausas, J. G., 2011: Mediterranean cork oak savannas require human use to sustain biodiversity and ecosystem services. Front. Ecol. Environ. **9**, 278–286.

Cameron, D. D.; Coats, A. M.; Seel, W. E., 2006: Differential resistance among host and non-host species underlies the variable success of the hemi-parasitic plant *Rhinanthus minor*. Ann. Bot. **98**, 1289–1299.

Camilo-Alves, C. D. E. P.; da Clara, M. I. E.; Ribeiro, N. M. C. D., 2013: Decline of Mediterranean oak trees and its association with *Phytophthora cinnamomi*: a review. Eur. J. For. Res. **132**, 411–432.

Chalmers, J. M.; Griffiths, P. R., 2002: Handbook of Vibrational Spectroscopy. Chichester: Wiley-Blackwell, pp. 3862.

Chen, D. W.; Zentmyer, G. A., 1970: Production of sporangia by *Phytophthora cinnamomi* in axenic culture. Mycologia **62**, 397–402.

Coates, J., 2000: Interpretation of infrared spectra, a practical approach. In: Encyclopedia of Analytical Chemistry. Ed. by Meyers, R. A. Chichester: Wiley-Blackwell, pp. 10815–10837.

Coelho, A. C.; Horta, M.; Ebadzad, G.; Cravador, A., 2011: *Quercus suber – Phytophthora cinnamomi* interaction: a hypothetical molecular mechanism model. N. Z. J. For. Sci. **41S**, S143–S157.

Conrad, A. O.; Rodriguez-Saona, L. E.; McPherson, B. A.; Wood, D. L.; Bonello, P., 2014: Identification of *Quercus agrifolia* (coast live oak) resistant to the invasive pathogen *Phytophthora ramorum* in native stands using Fourier-transform infrared (FT-IR) spectroscopy. Front. Plant Sci. **5**, 521.

Corcobado, T.; Solla, A.; Madeira, M. A.; Moreno, G., 2013: Combined effects of soil properties and *Phytophthora cinnamomi* infections on *Quercus ilex* decline. Plant Soil **373**, 403–413.

Corcobado, T.; Cubera, E.; Juárez, E.; Moreno, G.; Solla, A., 2014: Drought events determine performance of *Quercus ilex* seedlings and increase their susceptibility to *Phytophthora cinnamomi*. Agric. For. Meteorol. **192–193**, 1–8.

Cordeiro, N.; Belgacem, M. N.; Silvestre, A. J. D.; Neto, C. P.; Gandini, A., 1998: Cork suberin as a new source of chemicals. 1. Isolation and chemical characterization of its composition. Int. J. Biol. Macromol. **22**, 71–80.

Cots, F.; Tuset, J. J., 2002: Influence of culture water-solution of five species of Mediterranean *Quercus* in the asexual reproduction of *Phytophthora cinnamomi*. IOBC-WPRS Bull. **25**, 53–56.

De Jong, C. F.; Laxalt, A. M.; Bargmann, B. O. R.; de Wit, P.; Joosten, M.; Munnik, T., 2004: Phosphatidic acid accumulation is an early response in the Cf-4/Avr4 interaction. Plant J. **39**, 1–12.

Enkerli, K.; Hahn, M. G.; Mims, C. W., 1997: Immunogold localization of callose and other plant cell wall components in soybean roots infected with the oomycete *Phytophthora sojae*. Can. J. Bot. **75**, 1509–1517.

Fiehn, O., 2002: Metabolomics – the link between genotypes and phenotypes. Plant Mol. Biol. **48**, 155–171.

Gidman, E.; Goodacre, R.; Emmett, B.; Smith, A. R.; Gwynn-Jones, D., 2003: Investigating plant-plant interference by metabolic fingerprinting. Phytochemistry **63**, 705–710.

Hall, R. D., 2006: Plant metabolomics: from holistic hope, to hype, to hot topic. New Phytol. **169**, 453–468.

Hardham, A. R., 2005: *Phytophthora cinnamomi*. Mol. Plant Pathol. **6**, 589–604.

Horta, M.; Sousa, N.; Coelho, A. C.; Neves, D.; Cravador, A., 2008: *In vitro* and *in vivo* quantification of elicitin expression in *Phytophthora cinnamomi*. Physiol. Mol. Plant Pathol. **73**, 48–57.

Horta, M.; Caetano, P.; Medeira, C.; Maia, I.; Cravador, A., 2010: Involvement of the beta-cinnamomin elicitin in infection and colonisation of cork oak roots by *Phytophthora cinnamomi*. Eur. J. Plant Pathol. **127**, 427–436.

Hückelhoven, R., 2007: Cell wall associated mechanisms of disease resistance and susceptibility. Annu. Rev. Phytopathol. **45**, 101–127.

Jain, A.; Nandakumar, K.; Ross, A., 2005: Score normalization in multimodal biometric systems. Pattern Recognit. **38**, 2270–2285.

Jones, J. D. G.; Dangl, J. L., 2006: The plant immune system. Nature **444**, 323–329.

Kamnev, A. A.; Ristic, M.; Antonyuk, L. P.; Chernyshev, A. V.; Ignatov, V. V., 1997: Fourier transform infrared spectroscopic study of intact cells of the nitrogen-fixing bacterium *Azospirillum brasilense*. J. Mol. Struct. **408**, 201–205.

Kamoun, S.; van West, P.; Vleeshouwers, V.; de Groot, K. E.; Govers, F., 1998: Resistance of *Nicotiana benthamiana* to *Phytophthora infestans* is mediated by the recognition of the elicitor protein INF1. Plant Cell **10**, 1413–1425.

Kelley, B. S.; Lee, S. J.; Damasceno, C. M. B.; Chakravarthy, S.; Kim, B. D.; Martin, G. B.; Rose, J. K. C., 2010: A secreted effector protein (SNE1) from *Phytophthora infestans* is a broadly acting suppressor of programmed cell death. Plant J. **62**, 357–366.

Kim, J. K.; Bamba, T.; Harada, K.; Fukusaki, E.; Kobayashi, A., 2007: Time-course metabolic profiling in *Arabidopsis thaliana* cell cultures after salt stress treatment. J. Exp. Bot. **58**, 415–424.

Kozlowski, T. T., 1997: Responses of woody plants to flooding and salinity. Tree Physiol. **17**, 490–519.

Lanoue, A.; Burlat, V.; Henkes, G. J.; Koch, I.; Schurr, U.; Röse, U. S. R., 2010: *De novo* biosynthesis of defense root exudates in response to *Fusarium* attack in barley. New Phytol. **185**, 577–588.

Lecellier, A.; Mounier, J.; Gaydou, V.; Castrec, L.; Barbier, G.; Ablain, W.; Manfait, M.; Toubas, D.; Sockalingum, G. D., 2014: Differentiation and identification of filamentous fungi by high-throughput FTIR spectroscopic analysis of mycelia. Int. J. Food Microbiol. **168–169**, 32–41.

Logan, M., 2010: Biostatistical Design and Analysis Using R: A Practical Guide. Chichester: Wiley-Blackwell, pp. 576.

Martin, F.; Kamoun, S., 2012: Effectors in Plant-Microbe Interactions. Malaysia: Wiley-Blackwell, pp. 426.

Martin, J. A.; Solla, A.; Woodward, S.; Gil, L., 2007: Detection of differential changes in lignin composition of elm xylem tissues inoculated with *Ophiostoma novo-ulmi* using Fourier transform-infrared spectroscopy. For. Pathol. **37**, 187–191.

Martin, J. A.; Solla, A.; Coimbra, M. A.; Gil, L., 2008: Metabolic fingerprinting allows discrimination between *Ulmus pumila* and *U. minor*, and between *U. minor* clones of different susceptibility to Dutch elm disease. For. Pathol. **38**, 244–256.

Martín, J. A.; Solla, A.; Coimbra, M. A.; Gil, M., 2005: Metabolic distinction of *Ulmus minor* xylem tissues after inoculation with *Ophiostoma novo-ulmi*. Phytochemistry **66**, 2458–2467.

Medeira, C.; Quartin, V.; Maia, I.; Diniz, I.; Matos, M. C.; Semedo, J. N.; Scotti-Campos, P.; Ramalho, J. C.; Pais, I. P.; Ramos, P.; Melo, E.; Leitao, A. E.; Cravador, A., 2012: Cryptogein and capsicein promote defence responses in *Quercus suber* against *Phytophthora cinnamomi* infection. Eur. J. Plant Pathol. **134**, 145–159.

Moralejo, E.; Garcia-Munoz, J. A.; Descals, E., 2009: Susceptibility of Iberian trees to *Phytophthora ramorum* and *P. cinnamomi*. Plant. Pathol. **58**, 271–283.

Moreira, A. C.; Martins, J. M. S., 2005: Influence of site factors on the impact of *Phytophthora cinnamomi* in cork oak stands in Portugal. For. Pathol. **35**, 145–162.

Morris, V. J.; Ring, S. G.; MacDougall, A. J.; Wilson, R. H., 2003: Biophysical characterization of plant cell walls. In: The Plant Cell Wall. Ed. by Rose, J. K. C. Boca Raton, USA: CRC Press, pp. 55–94.

Myers, N.; Mittermeier, R. A.; Mittermeier, C. G.; da Fonseca, G. A. B.; Kent, J., 2000: Biodiversity hotspots for conservation priorities. Nature **403**, 853–858.

Oßwald, W.; Fleischmann, F.; Rigling, D.; Coelho, A. C.; Cravador, A.; Diez, J.; Dalio, R. J.; Horta Jung, M.; Pfanz, H.; Robin, C.; Sipos, G.; Solla, A.; Cech, T.; Chambery, A.; Diamandis, S.; Hansen, E.; Jung, T.; Orlikowski, L. B.; Parke, J.; Prospero, S.; Werres, S., 2014: Strategies of attack and defence in woody plant–*Phytophthora* interactions. For. Pathol. **44**, 169–190.

Pinto-Correia, T.; Godinho, S., 2013: Changing agriculture-changing landscape: what is going on in the high nature valued Montado landscapes of southern Portugal. In: Agriculture in Mediterranean Europe: Between Old and New Paradigms. Ed. by Ortiz-Miranda, D.; Moragues-Faus, A.; Arnalte-Alegre, E. Bingley: Emerald Group Publishing, pp. 75–90.

Pinto-Correia, T.; Menezes, H.; Barroso, L. F., 2014: The landscape as an asset in southern european fragile agricultural systems: contrasts and contradictions in land managers attitudes and practices. Landsc. Res. **39**, 205–217.

Pollard, M.; Beisson, F.; Li, Y.; Ohlrogge, J. B., 2008: Building lipid barriers: biosynthesis of cutin and suberin. Trends Plant Sci. **13**, 236–246.

Pugin, A.; Frachisse, J. M.; Tavernier, E.; Bligny, R.; Gout, E.; Douce, R.; Guern, J., 1997: Early events induced by the elicitor cryptogein in tobacco cells: involvement of a plasma membrane NADPH oxidase and activation of glycolysis and the pentose phosphate pathway. Plant Cell **9**, 2077–2091.

Qutob, D.; Kamoun, S.; Gijzen, M., 2002: Expression of a *Phytophthora sojae* necrosis-inducing protein occurs during transition from biotrophy to necrotrophy. Plant J. **32**, 361–373.

R Core Team, 2013. R Foundation for Statistical Computing. Vienna: Austria. http://www.R-project.org/.

Robin, C.; Capron, G.; Desprez-Loustau, M. L., 2001: Root infection by *Phytophthora cinnamomi* in seedlings of three oak species. Plant. Pathol. **50**, 708–716.

Spiteller, G., 2003: The relationship between changes in the cell wall, lipid peroxidation, proliferation, senescence and cell death. Physiol. Plant. **119**, 5–18.

Stuart, B. H., 2004: Infrared Spectroscopy: Fundamentals and Applications. Chichester: John Wiley & Sons, pp. 242.

Taoutaou, A.; Socaciu, C.; Pamfil, D.; Fetea, F.; Balazs, E.; Botez, C., 2012: New markers for potato late blight resistance and susceptibility using FTIR spectroscopy. Not. Bot. Horti. Agrobot. **40**, 150–154.

Testerink, C.; Munnik, T., 2005: Phosphatidic acid: a multifunctional stress signaling lipid in plants. Trends Plant Sci. **10**, 368–375.

Thomas, R.; Fang, X.; Ranathunge, K.; Anderson, T. R.; Peterson, C. A.; Bernards, M. A., 2007: Soybean root suberin: anatomical distribution, chemical composition, and relationship to partial resistance to *Phytophthora sojae*. Plant Physiol. **144**, 299–311.

Torres, M. A.; Jones, J. D. G.; Dangl, J. L., 2006: Reactive oxygen species signaling in response to pathogens. Plant Physiol. **141**, 373–378.

Tyler, B. M., 2002: Molecular basis of recognition between *Phytophthora* pathogens and their hosts. Annu. Rev. Phytopathol. **40**, 137–167.

Underwood, W., 2012: The plant cell wall: a dynamic barrier against pathogen invasion. Front. Plant Sci. **3**, 85.

Vanholme, R.; Demedts, B.; Morreel, K.; Ralph, J.; Boerjan, W., 2010: Lignin biosynthesis and structure. Plant Physiol. **153**, 895–905.

Vega-Sanchez, M. E.; Redinbaugh, M. G.; Costanzo, S.; Dorrance, A. E., 2005: Spatial and temporal expression analysis of defense-related genes in soybean cultivars with different levels of partial resistance to *Phytophthora sojae*. Physiol. Mol. Plant Pathol. **66**, 175–182.

Vivas, M.; Nunes, C.; Coimbra, M. A.; Solla, A., 2014: Maternal effects and carbohydrate changes of *Pinus pinaster* after inoculation with *Fusarium circinatum*. Trees **28**, 373–379.

Wang, X.; Devaiah, S. P.; Zhang, W.; Welti, R., 2006: Signaling functions of phosphatidic acid. Prog. Lipid Res. **45**, 250–278.

Wehrens, R., 2011: Chemometrics with R: Multivariate Data Analysis in the Natural Sciences and Life Sciences. Heidelberg, DE: Springer, pp. 285.

Supporting Information

Additional Supporting Information may be found in the online version of this article:

Figure S1. Heatmap of FT-IR bands from roots of *Quercus suber.*

Figure S2. Heatmap of FT-IR bands from mycelium of *Phytophthora cinnamomi*.

Table S1. (a) Correlation table of absorbance values of FT-IR bands from *Quercus suber* roots challenged with *Phytophthora cinnamomi* when subtracted from the absorbance values of FT-IR bands of mock-inoculated *Q. suber* roots. (b) Corresponding statistical values (*q*-values) obtained from the correlation table (Table S1a).

Table S2. (a) Correlation table of the absorbance values of FT-IR bands from *Phytophthora cinnamomi* when exposed to *Quercus suber* root exudates after subtracting the absorbance values of FT-IR bands from mock-exposed *P. cinnamomi* mycelium. (b) Corresponding statistical values (*q*-values) obtained from the correlation table (Table S2a).